
Volume 1 | Number 1 | Jan 2013 | Pages 1–100
Dalton Transactions
An international journal of inorganic chemistry
www.rsc.org/dalton
ROYAL SOCIETY OF CHEMISTRY

Table of contents entry

Two ferrocene-isocoumarin conjugated molecules, **Fc-Icm** and **BFc-PIcm**, have been synthesized through the acid-prompted regioselective oxidative cyclization from the corresponding ferrocenylethynyl terephthalates. Their electronic structure, redox properties and UV−vis spectra are in good agreement with the DFT and TDDFT calculations.

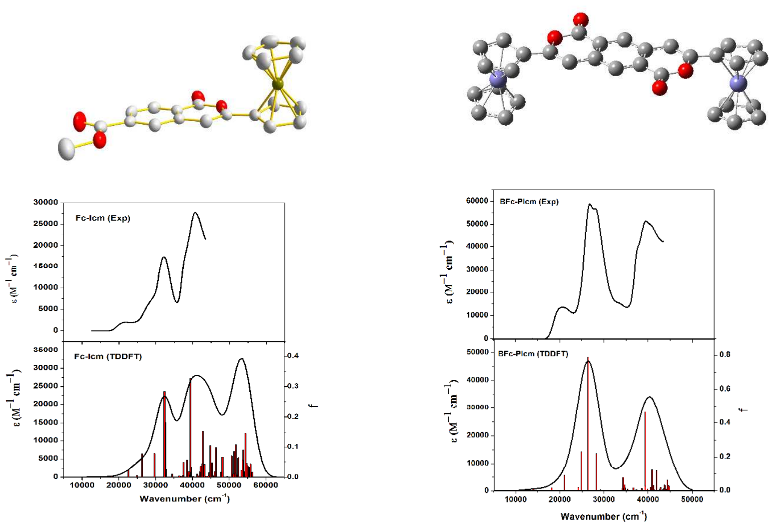

Ferrocene-Isocoumarin Conjugated Molecules: Synthesis, Structural Characterization, Electronic Properties, and DFT-TDDFT Computational Study

Ye-Dong Peng[a], Lin-Sen Zhou[b], Li-Li Chen[a], Lu Ma[a], Yue Zhao[a], Wen-Wei Zhang*[a], Jing-Lin Zuo[a]

[a] *Institute of Coordination Chemistry, State Key Laboratory of Coordination Chemistry, School of Chemistry and Chemical Engineering, Nanjing University, Nanjing 210093, People's Republic of China. E-mail: wwzhang@nju.edu.cn.*

[b] *Institute of Theoretical and Computational Chemistry, Key Laboratory of Mesoscopic Chemistry, School of Chemistry and Chemical Engineering, Nanjing University, Nanjing 210093, People's Republic of China*

Abstract

Two ferrocene-isocoumarin conjugated molecules, methyl 3-ferrocenyl-1-oxo-1H-isochromene-6-carboxylate (**Fc-Icm**) and 3,8-bisferrocenylpyrano[3,4-g]isochromene -1,6-dione (**BFc-PIcm**), have been synthesized through the acid-prompted regioselective oxidative cyclization from dimethyl 2-(ferrocenylethynyl)terephthalate (**Fc-TP**) and dimethyl 2,5-bis(ferrocenylethynyl)terephthalate (**BFc-TP**), respectively. Single-crystal X-ray diffraction, together with the density functional theory (DFT) calculations, shows that the ferrocene-isocoumarin conjugated compounds display better coplanarity than the corresponding ferrocenylethynyl terephthalates. All the compounds exhibit characteristic MLCT, ICT and π-π* transitions in the UV-visible range in solution, and **Fc-Icm** and **BFc-PIcm** show higher oscillator strength of the absorption compared with **Fc-TP** and **BFc-TP**, which are verified by time-dependent DFT (TDDFT) theoretical calculations. The electrochemical properties are studied by cyclic voltammetry (CV), which are also in accord with the theoretical calculations.

Keywords: ferrocene, isocoumarin, conjugated molecule, electrochemical property, DFT and TDDFT theoretical calculation

Introduction

Molecules with extending π-electron conjugated system are promising candidates for nanoscale devices and switches due to their unique properties in electrical, optical and magnetic fields, which have attracted wide attention and deep research in recent decades.[1] Usually, functional building blocks, linkers bridging the building units, and the molecular geometry in the extending π-electron systems have prominent influence on the electrical and optical properties.[2] Therefore, the contriving of novel conjugated molecules are essential for investigating the electronic and optoelectronic properties of such materials and further improving the performance of these devices.

Ferrocene substituents with unique redox properties are found to be potentially useful in generating semiconductor, superconductor, molecular sensors, light-harvesting assemblies, magnetic, NLO, and redox catalyst materials, etc,[3] and they often serve as the building blocks in the construction of π-conjugated system.[4] On the other hand, isocoumarin is a kind of conjugated heterocyclic compound with high coplanarity, its skeleton is found in a variety of natural products, and it is an important building unit in many biological and material molecules.[5] Isocoumarin derivatives show various biological and physiological activities, such as antibacterial, antifungal, anticancer, antidiabetic, phytotoxic, and protease inhibition activities.[6] Therefore, much attention has been paid to the relevant study on the biological study, and also some work are detailed on the regioselective construction of isocoumarins through different methods.[7] Until now, most of the isocoumarin derivatives synthesized and studied are organic compounds, few examples have been accessed to the isocoumarin compounds containing organometallic units. Considering the remarkable properties of ferrocene and isocoumarin, and that both the electron-rich ferrocenyl unit (donor, D) and the electron-deficient isocoumarin ring (acceptor, A) are excellent molecular building blocks for the highly extending π-electron conjugations, new π-extending system containing both of them are attempted to synthesize. These D-A ferrocene-isocoumarin molecules, methyl 3-ferrocenyl-1-oxo-1H-isochromene -6-carboxylate (**Fc-Icm**) and 3,8-ferrocenylpyrano[3,4-g]isochromene-1,6-dione (**BFc-PIcm**), together with the intermediate products, dimethyl 2-(ferrocenylethynyl)terephthalate (**Fc-TP**) and dimethyl 2,5-bis(ferrocenylethynyl)terephthalate (**BFc-TP**), are shown in **Scheme 1**. The single-crystal and electronic structure, electronic and electrochemical properties of them are investigated. Detailed results and discussion are elaborated in the following sections.

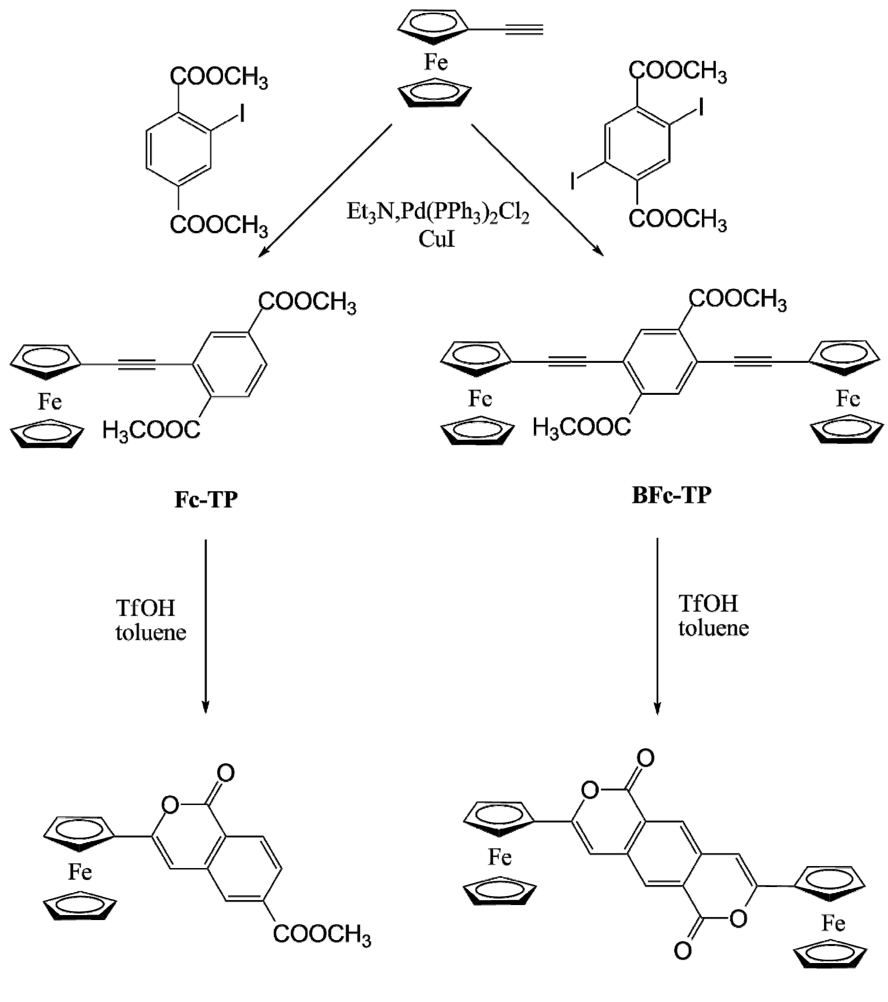

Scheme 1. Synthetic procedure of **Fc-Icm** and **BFc-PIcm**.

Experimental

General

All chemicals were purchased as reagent grade and used without further purification. Dichloromethane, triethylamine and toluene were dried and distilled according to standard procedures. Dimethyl 2-iodoterephthalate[8] and dimethyl 2,5-diiodoterephthalate[9] were prepared according to literature procedures. All of the reactions were monitored by TLC. Silica gel (100-200 mesh) was used for column chromatography. Elemental analyses (C, H) were carried out on a Perkin-Elmer 240 analyzer. The IR spectra were obtained on a VECTOR TM 22 spectrometer with KBr pellets in the 4000-400 cm^{-1} region, the electronic absorption spectra were carried out on a LAMBDA-35 UV/vis spectrophotometer, and ^{1}H and ^{13}C NMR spectra were measured on a Bruker DRX-500 spectrometer at 298 K using TMS as the internal standard. The MALDI-TOF-MS spectra were recorded on a Bruker Daltonics flexAnalysis autoflex TOF/TOF spectrometer using α-cyano-4-hydroxycinnamic acid (HCCA) as matrix.

Synthesis of Fc-TP. Under an N_2 atmosphere, a suspension of dimethyl 2-iodoterephthalate (0.320 g, 1.00 mmol) and ethynylferrocene (0.252 g, 1.20 mmol), together with bis (triphenylphosphine) palladium(II) dichloride (0.020 g, 0.014 mmol) and copper(I) iodide (0.009 g, 0.05 mmol) in anhydrous triethylamine (10 mL), was stirred and heated to reflux temperature until complete consumption of the iodide (monitored by TLC). Then the solvent was evaporated under vacuum. The residue was dissolved in dichloromethane, washed with water for several times, dried with anhydrous $MgSO_4$, and then filtered off. The product in the filtrate was chromatographed on silica gel using ethyl acetate–petroleum ether (1/6 v/v) as eluent. The second yellow band was collected and then evaporated under vacuum to give a yellow solid. Yield: 0.373 g (92.8 %). Crystals of **Fc-TP** suitable for an X-ray structural determination were obtained by slow evaporation of a mixed ethyl acetate-petroleum ether solution of **Fc-TP**. IR (KBr disk): 2220 cm^{-1} ($\nu_{C\equiv C}$), 1722 cm^{-1} ($\nu_{C=O}$). ^{1}H NMR (500 MHz, $CDCl_3$): δ (ppm) 8.23 (s, 1H), 8.10 (s, 1H), 7.96 (s, 1H), 4.59 (s, 2H), 4.32 (s, 7H), 3.99 (s, 3H), 3.96 (s, 3H). ^{13}C NMR (500 MHz, $CDCl_3$): δ (ppm) 52.46 (CH_3), 52.66 (CH_3), 64.76 (Cp), 69.36 (Cp), 70.21 (Cp), 71.79 (Cp), 83.90 (C≡C), 95.34 (C≡C), 124.83 (Ph), 127.90 (Ph), 129.68 (Ph), 130.53 (Ph), 132.97 (Ph), 134.88 (Ph), 165.91 (C=O), 166.39 (C=O). Anal. Calcd for $C_{22}H_{18}O_4Fe$: C, 65.69; H, 4.51. Found: C, 65.47; H, 4.54; MS: *m/z* 401.6 (M^+) (calcd 402.06).

Synthesis of Fc-Icm. Under an N_2 atmosphere, trifluoromethane sulfonic acid (TfOH, 0.09 mL, 1.00 mmol) was dropped slowly to a solution of **Fc-TP** (0.402 g, 1.00 mmol) in toluene (25 mL). During the dropping process, the reaction mixture was stirred and heated to reflux temperature until complete consumption of **Fc-TP** (monitored by TLC). Then the solvent was evaporated under vacuum until almost dried. After that, the residue was chromatographed on silica gel using ethyl acetate-petroleum ether (1/6 v/v) as eluent. The first orange-red band was collected and then evaporated under vacuum to give an orange-red solid. Yield: 0.348 g (84.7 %). Crystals of **Fc-Icm** suitable for an X-ray structural determination were obtained by slow evaporation of an ethyl acetate-petroleum ether solution of **Fc-Icm**. IR (KBr disk): 1729 cm^{-1} ($\nu_{C=O}$), 1640 cm^{-1} ($\nu_{C=C}$); ^{1}H NMR (500 MHz, $CDCl_3$): δ (ppm) 8.31 (d, J=10.0Hz, 1H), 8.06 (s, 1H), 8.03 (d, J=5.0Hz, 1H), 6.56 (s, 1H), 4.87 (s, 2H), 4.51 (s, 2H), 4.24 (s, 5H), 3.98 (s, 3H). ^{1}C NMR (500 MHz, $CDCl_3$): δ (ppm) 52.81 (CH_3), 66.65 (Cp), 70.12 (Cp), 70.62 (Cp), 76.49 (Cp), 99.35 (Icm), 122.80 (Icm), 126.74 (Icm), 127.17 (Icm), 130.21 (Icm), 135.90 (Icm), 138.19 (Icm), 157.68 (Icm), 161.99 (Icm), 166.05 (C=O). Anal. Calcd for $C_{21}H_{16}O_4Fe$: C, 64.97; H, 4.15. Found: C, 64.66; H, 4.46; MS: *m/z* 387.5 (M^+) (calcd 388.04).

Synthesis of BFc-TP. Under an N_2 atmosphere, a suspension of dimethyl 2,5-diiodoterephthalate (0.446 g, 1.00 mmol) and ethynylferrocene (0.630 g, 3.00 mmol), together with bis(triphenylphosphine)palladium(II) dichloride (0.036 g, 0.05 mmol) and copper(I) iodide (0.009 g, 0.05 mmol) in anhydrous triethylamine (30 mL), was stirred and heated to reflux temperature until complete consumption of the iodide (monitored by TLC). Then the solvent was evaporated under vacuum. The residue was dissolved in dichloromethane and this solution was washed with water for several times, dried with anhydrous $MgSO_4$. After filtration and concentration, the desired product **BFc-TP** was separated by column chromatography on silica gel using dichloromethane as eluent. Yield: 0.345 g (56.7 %). IR (KBr disk): 2210 cm^{-1} ($\nu_{C\equiv C}$), 1732 cm^{-1} ($\nu_{C=O}$); ^{1}H NMR (500 MHz, $CDCl_3$): δ (ppm) 8.11 (s, 2H), 4.57 (s, 4H), 4.32 (s, 4H), 4.31 (s, 10H), 4.00 (s, 6H). ^{13}C NMR (500 MHz, $CDCl_3$): δ (ppm) 52.59 (CH_3), 64.77 (Cp), 69.50 (Cp), 70.28 (Cp), 71.86 (Cp), 84.20 (C≡C), 96.79 (C≡C), 122.98 (Ph), 134.10 (Ph), 135.79 (Ph), 165.94 (C=O). Anal. Calcd for $C_{34}H_{26}O_4Fe_2$: C, 66.92; H, 4.29. Found: C, 66.90; H, 4.32; MS: *m/z* 609.4 (M^+) (calcd 610.05).

Synthesis of BFc-PIcm. Under an N_2 atmosphere, trifluoromethane sulfonic acid (TfOH, 0.18 mL, 2.00 mmol) was dropped slowly to a solution of **BFc-TP** (0.61 g, 1.00 mmol) in toluene (30 mL). During the dropping process, the reaction mixture was stirred and heated to reflux temperature until complete consumption of **BFc-TP** (monitored by TLC). Then the solvent was evaporated under vacuum to dryness. After that, the residue was chromatographed on silica gel using dichloromethane as eluent. Yield: 0.124 g (21.3 %). IR (KBr disk): 1721 cm^{-1} ($\nu_{C=O}$), 1633 cm^{-1} ($\nu_{C=C}$); ^{1}H NMR (500 MHz, $CDCl_3$): δ (ppm) 8.28 (s, 2H), 6.59 (s, 2H), 4.87 (s, 4H), 4.51 (s, 4H), 4.24 (s, 10H). ^{13}C NMR (500 MHz, $CDCl_3$): δ (ppm) 66.95 (Cp), 70.64 (Cp), 71.20 (Cp), 99.47 (PIcm), 125.00 (PIcm), 126.90 (PIcm), 135.69 (PIcm), 156.86 (PIcm), 161.81 (PIcm). Anal. Calcd for $C_{32}H_{22}O_4Fe_2$: C, 66.01; H, 3.81. Found: C, 65.98; H, 3.84; MS: *m/z* 581.5 (M^+) (calcd 582.02).

Electrochemical measurements

Cyclic voltammetric experiments were performed under nitrogen in dry and degassed CH_2Cl_2 at a scan rate of 100 mV s^{-1} with a CHI 660B potentiostatic instrument at room temperature. The three-electrode cell comprises a 1 mm platinum-disk working electrode, a platinum-wire auxiliary electrode, and an Ag/Ag^+ reference electrode. The electrolyte is n-Bu_4NClO_4 (0.1 mol L^{-1}). The potentials were corrected to the internal standard of Fc/Fc^+ in CH_2Cl_2.

DFT and TDDFT calculations

The ground-state geometries of all compounds were fully optimized using the density functional theory (DFT), with the B3LYP exchange-correlation functional[10, 11] and LANL2DZ[12] basis sets. All calculations were carried out with the Gaussian 09 program.[13] The time-dependent density functional theory (TDDFT) calculations of the excitation energies were then performed at the optimized geometries of the ground states.

X-ray structural analysis

Single crystal X-ray diffraction data were collected on a Bruker Smart Apex II CCD diffractionmeter at 291 K using graphite monochromated Mo/Kα radiation (λ=0.71073 Å). Data reductions and absorption corrections were performed with the SAINT and SADABS software packages,[14] respectively. Structures were solved by a direct method using the SHELXL-97 software package.[15] The non-hydrogen atoms were anisotropically refined using the full-matrix least-squares method on F^2. All hydrogen atoms were placed at the calculated positions and refined riding on the parent atoms. The crystallographic data for **Fc-TP** and **Fc-Icm** are listed in **Table 1**. The CCDC reference numbers for them are 1060479 and1060478, respectively.

Table 1 Summary of Crystallographic Data for **Fc-TP** and **Fc-Icm**

	Fc-TP	**Fc-Icm**
Empirical formula	$C_{22}H_{18}FeO_4$	$C_{21}H_{16}FeO_4$
Formula weight	402.21	388.19
Crystal system	monoclinic	triclinic
Space group	$P2_1/c$	$P\bar{1}$
a (Å)	12.984 (5)	6.9465 (11)
b (Å)	7.585 (3)	11.1130 (18)
c (Å)	19.439 (7)	11.4780 (19)
α (º)	90	104.735 (3)
β (º)	109.046 (7)	92.002 (3)
γ (º)	90	99.764 (2)
V(Å^3)	1809.6 (12)	841.7 (2)
Z	4	2
ρ (g/cm^3)	1.476	1.532
μ (mm^{-1})	0.859	0.920
θ range (º)	2.22-26.00	1.84-25.01
GOF^a	1.045	1.054
$R_1{}^b$, $wR_2{}^c$[I>2σ(I)]	0.0477, 0.0857	0.0404, 0.1023
R_1 , wR_2 (all data)	0.0651, 0.0881	0.0598, 0.1110

^{a}GOF = $\Sigma[w(F_o^2-F_c^2)^2]/(n-p)^{1/2}$, where n is the number of data and p is the number of parameters refined.

$^bR_1 = \Sigma||F_0|-|F_c|/\Sigma|F_0|$; $^cwR_2 = \{\Sigma[w(F_0^2-F_c^2)^2]/\Sigma[w(F_0^2)^2]\}^{1/2}$.

Results and discussion

Synthesis and structural characterization

Scheme 1 describes the synthetic procedures and the structures of the main intermediates and the respective products. The target ferrocene-isocoumarin conjugated molecules **Fc-Icm** and **BFc-Icm** were synthesized from regioselective intramolecular cyclization of the corresponding ferrocenylethynyl terephthalates **Fc-TP** and **BFc-TP** in the presence of trifluoromethane sulfonic acid (TfOH),[7d] which were synthesized by the Sonogashira cross-coupling reaction from ethynylferrocene with iodoterephthalate or diiodoterephthalate using bis-(triphenylphosphine)palladium(II) and copper(I) iodide as catalysts and triethylamine as a base. All the compounds were fully characterized by IR, ^{1}H NMR spectra, MS, and element analysis. All the results given in the experimental section were in good accordance with the proposed structures. For instance, from IR spectra, besides the characteristic -C=O- stretching vibrations around 1730 cm^{-1}, the ferrocenylethynyl terephthalate intermediate compounds **Fc-TP** and **BFc-TP** also exhibit the characteristic -C≡C- stretching vibrations around 2200 cm^{-1}, while the target ferrocene-isocoumarin conjugated molecules **Fc-Icm** and **BFc-Icm** display the characteristic -C=C- stretching vibrations around 1640 cm^{-1}. And, in comparison the ^{1}H NMR and ^{13}C NMR spectra of the ferrocene-isocoumarin compounds with those of the corresponding ferrocenylethynyl terephthalates, it can be found that a new characteristic resonance band around 6.6 ppm emerged in the ^{1}H NMR spectra for the ferrocene-isocoumarin compounds, and the characteristic -C≡C- resonance peak in the range of 83-97 ppm disappeared in the ^{13}C NMR spectra after intramolecular cyclization of the ferrocenylethynyl terephthalates, all above indicate the formation of the pyrano moiety upon cyclization of the aromatic carboxylate with the alkynyl group. Moreover, the MS and the analytical data also verify that the synthesized complexes are in agreement with the predicted molecular structures. Fortunately, good crystallographic data were obtained for compounds **Fc-TP** and **Fc-Icm**, further identifying the regiocontrolled intramolecular cyclization of ferrocenylethynyl terephthalates**.** The molecular structures of **Fc-TP** and **Fc-Icm** are shown in **Fig. 1**, and some selected bond lengths and angles are given in **Table 2**.

Fc-TP crystallizes in the $P2_1/c$ space group. The C≡C, C=O and C-O bond lengths are within the expected range (C11-C12 = 1.181Å, C19-O1 = 1.170Å, C21-O3 = 1.191 Å, C19-O2 = 1.302 Å, C21-O4 = 1.326 Å), and the -C≡C- bond angle is nearly 180° (C1-C11-C12 = 179.7°, C11-C12-C13 = 175.0°). The two Cp rings of the ferrocenyl group are almost parallel to each other (the dihedral angle of Cp1 and Cp2 is only 1.0°). The phenyl ring (Ph) is nearly perpendicular to the adjacent Cp1 (the dihedral angle of Cp1 and Ph is 81.2°). Adjacent molecules in **Fc-TP** are stacked in an inverse fashion along the *b* axis, resulting in intramolecular (C6-H6···O2 = 3.336 Å) and intermolecular hydrogen bonds (C2-H2···O4 = 3.315 Å) in it, which can be clearly seen in **Fig. S2** and **Table S1**.

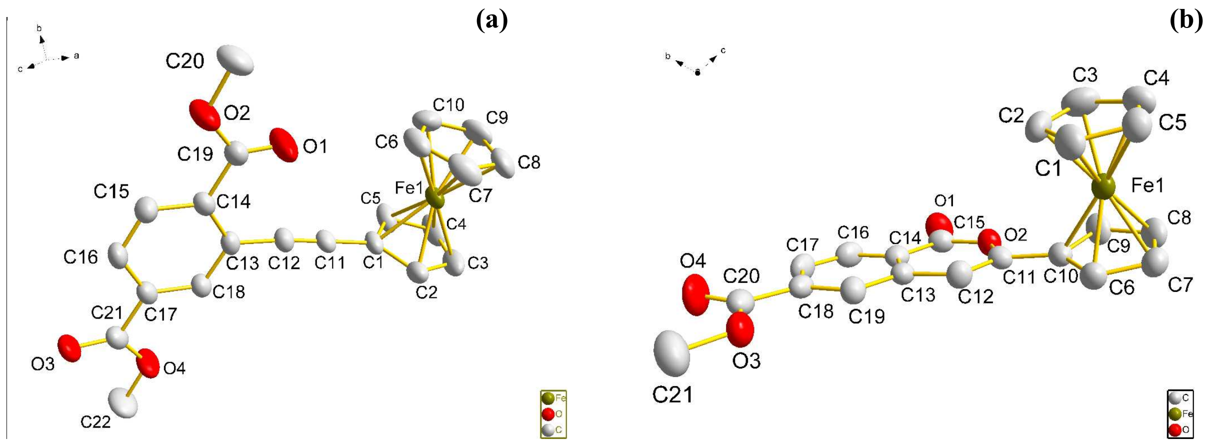

Fig. 1 Crystal structure of (a) **Fc-TP** and (b) **Fc-Icm** with ellipsoids set at the 50% probability level. Hydrogen atoms are omitted for clarify.

Table 2 Selected bond lengths (Å) and angles (^{o}) for **Fc-TP** and **Fc-Icm**

		Fc-TP	
C1-C11	1.426 (45)	C11-C12	1.181 (45)
C12-C13	1.437 (44)	C13-C14	1.400 (38)
C14-C19	1.488 (43)	C19-O1	1.170 (54)
C19-O2	1.302 (39)	C21-O3	1.191 (40)
C21-O4	1.326 (37)		
C1-C11-C12	179.7 (304)	C11-C12-C13	175.0 (300)
		Fc-Icm	
C10-C11	1.464 (52)	C11-C12	1.329 (54)
C12-C13	1.444 (51)	C13-C14	1.393 (47)
C14-C15	1.461 (54)	C15-O1	1.201 (43)
C15-O2	1.380 (43)	C11-O2	1.379 (39)
C20-O3	1.324 (47)	C20-O4	1.191 (51)
C11-C12-C13	120.4 (313)	C12-C13-C14	118.4 (312)
C13-C14-C15	120.3 (313)	C14-C15-O2	116.9 (283)
O2-C11-C12	121.8 (312)	C15-O2-C11	122.3 (258)
C10-C11-C12	126.4 (316)		

Fc-Icm crystallizes in the $P\bar{1}$ space group. As shown in **Table 2**, both the C=C and C-O bond lengths (C11-C12 = 1.330 Å, C11-O2 = 1.379 Å, C15-O2 = 1.380 Å) formed after intramolecular cyclization and the C-C-C, C-C-O and C-O-C bond angles (116.9~122.3°) of the pyrano ring are within the expected range, clearly indicating the formation of the pyrano moiety. Two Cp rings in the ferrocenyl moiety are also nearly parallel to each other (the dihedral angle of them is 2.8°). The dihedral angle between benzo and pyrano ring is only 1.9°, thus the isocoumarin (Icm) skeleton could be regarded as coplanar. Besides, the dihedral angle between Icm and the adjacent Cp is only 10.6°, suggesting better coplanarity compared with **Fc-TP**. Strong offset π-π stacking interactions exist in **Fc-Icm**, with a centroid-to-centroid distance of 3.657 Å (**Fig. S3**). Whereas, only one kind of intermolecular hydrogen bond (C2-H2···O4 = 3.320 Å) is observed in **Fc-Icm** (**Fig. S4**), the relevant parameters are also listed in **Table S1**.

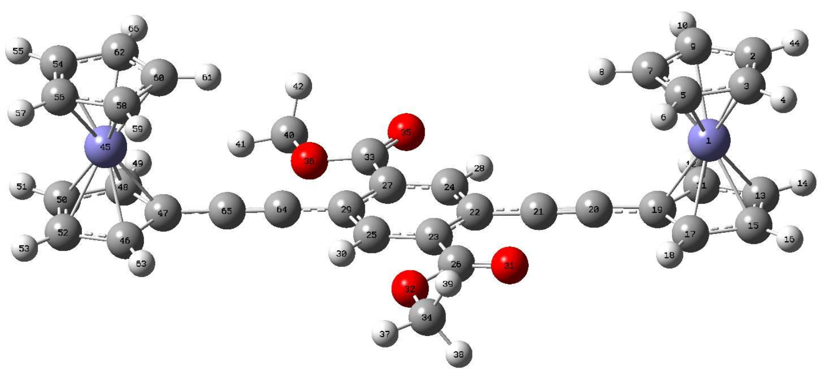

BFc-TP

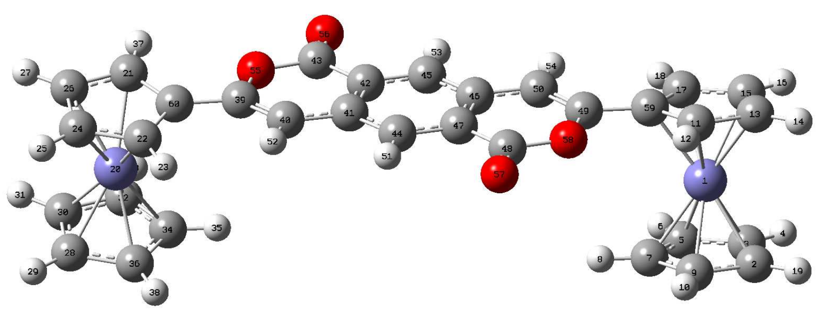

BFc-PIcm

Fig. 2 Optimized ground-state geometries of **BFc-TP** and **BFc-PIcm** with *cis*-structure as predicted by DFT calculations.

Since the crystal structures of **BFc-TP** and **BFc-PIcm** were not obtained, we turn to study the optimized ground-state geometries obtained by quantum chemical calculations. It is worth to mention that the data of the optimized ground-state geometry obtained by quantum chemical calculation are reasonably close to the single crystal data since we also get the calculated geometry data of **Fc-TP** and **Fc-Icm** using the same method, which can be clearly seen in **Table S2**. Moreover, it should be noted that both *cis*- and *trans*-structure maybe exist for the biferrocenyl compounds of **BFc-TP** and **BFc-PIcm** since the *cis*- and *trans*-form have approximate single-point energy from the DFT calculations (the single-point energy of *cis*-/*trans*-**BFc-TP** is -1858.67168412/-1858.67174410 a.u., of *cis*-/*trans*-**BFc-PIcm** is -1780.18358382/-1780.18350642 a.u.), and the molecular orbital energy and compositions of the two different forms are also very close. Only the results of *cis*-structure are given below (**Fig. 2** and **Table 3**). The DFT and TDDFT calculations of them with *trans*-form are given in the supporting information (**Fig. S5-S7**, **Table S3-S7**).

Some main bond lengths, bond angles and torsion angles of **BFc-TP** and **BFc-PIcm** with *cis*-form predicted by DFT calculations are shown in **Table 3**. In *cis*-**BFc-TP**, the -C≡C- bond length is 1.227 Å, a little longer than that in **Fc-TP** and the unconjugated molecules. The C−C bond length next to the ethynylene bond is 1.420 Å, a little shorter than the common C−C bond length. In addition, the -C≡C- bond angle almost displays linearity (C19-C20-C21, 176.4°; C20-C21-C22, 176.9°), and the phenyl (Ph) ring and Cp ring are nearly coplanar, since the torsion angles between Ph and Cp are nearly 180°/0° (C27-C29-C47-C46, 177.8°; C27-C29-C47-C48, -3.0°; C11-C19-C22-C23, -179.7°; C11-C19-C22-C24, 0.6°), which is quite different from that in **Fc-TP**. Thus *cis*-**BFc-TP** has better coplanarity compared with **Fc-TP**. In *cis*-**BFc-PIcm**, the C=C bond length is 1.366 Å, similar with the normal bond length. The C−C bond linking the ferrocenyl and pyrano unit is 1.445 Å, a little shorter than the common C−C bond length. Just like those in **Fc-Icm**, the benzo ring and the two pyrazo rings in *cis*-**BFc-PIcm** are almost in the same plane (C43-C42-C41-C44, -179.9°; C45-C46-C47-C48, -180°), and the pyrano ring and the Cp ring can also be considered as coplanarity (C21-C60-C39-C40, 169.5°; C17-C59-C49-C50， -10.4°). So it is obvious that the π electrons in *cis*-**BFc-TP** and *cis*-**BFc-PIcm** will be delocalized. Similar results can be obtained for the *trans*-**BFc-TP** and *trans*-**BFc-PIcm** compounds from the torsion angles shown in **Table S3**. Moreover, there are more conjugated units and a slightly better coplanarity in **BFc-TP** and **BFc-PIcm**, enabling better electronic coupling between Fc and Ph/Icm units and resulting in superior conjugated effect in the ground state of **BFc-TP** and **BFc-PIcm**, which can satisfactorily rationalize the experimental photo- and electrochemical properties detailed below.

Table 3 Selected bond lengths (Å), angles (^{o}) and torsion angles (^{o}) of **BFc-TP** and **BFc-PIcm** with *cis*-form predicted by DFT calculations

	cis-**BFc-TP**		
C19-C20	1.418	C20-C21	1.227
C21-C22	1.425	C29-C64	1.428
C64-C65	1.227	C65-C47	1.420
C19-C20-C21	176.4	C20-C21-C22	176.9
C29-C64-C65	174.0	C64-C65-C47	178.3
C27-C29-C47-C48	-3.0	C27-C29-C47-C46	177.8
C11-C19-C22-C24	0.6	C11-C19-C22-C23	-179.7
	cis-**BFc-PIcm**		
C49-C59	1.455	C49-C50	1.366
C46-C50	1.445	C39-C60	1.455
C39-C40	1.366	C40-C41	1.445
C21-C60-C39-C40	169.5	C43-C42-C41-C44	-179.9
C45-C46-C47-C48	-180.0	C17-C59-C49-C50	-10.4

Electronic properties

The solution-phase UV-vis absorption spectra of all compounds were recorded at room temperature. The absorption spectra reported in **Fig. 3** are dominated in the UV-visible region by absorption features at about 230-250, 300-360, 360-410 and 440-500 nm, which are given in **Table 4**. Generally, these bands can be assigned to π-π*, ICT (intramolecular charge transfer) and MLCT (metal-to-ligand charge transfer) transitions, mixed with some d–d character.[16] The corresponding computational study will be discussed later and give a detailed band assignment.

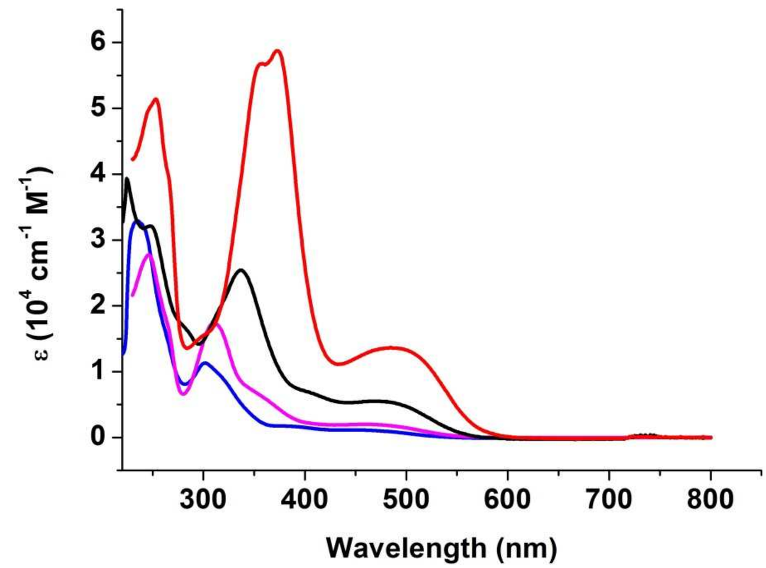

Fig. 3 UV-vis absorption spectra of **Fc-TP** (blue), **Fc-Icm** (magenta), **BFc-TP** (black) and **BFc-PIcm** (red) in dichloromethane at room temperature.

Table 4 UV-Vis absorption properties of **Fc-TP**, **Fc-Icm**, **BFc-TP** and **BFc-PIcm** in CH_2Cl_2

Complex	λ_{max} (nm) (ε (10^4 M^{-1} cm^{-1}))				
Fc-TP	235 (3.30)	302 (1.13)	382 (0.17)	464 (0.11)	
Fc-Icm	246 (2.77)	311 (1.74)	357 (0.63)	445 (0.20)	
BFc-TP	225 (3.94)	247 (3.22)	336 (2.54)	408 (0.67)	473 (0.55)
BFc-PIcm	247 (5.14)	358 (5.68)	372 (5.88)	483 (1.45)	

From **Fig. 3** and **Table 4**, together with the TDDFT data given below, it can be seen clearly that the π-π*, ICT and MLCT transitions of the biferrocenyl products **BFc-TP** and **BFc-PIcm** are bathochromically shifted compared with those of the monoferrocenyl compounds **Fc-TP** and **Fc-Icm**. Moreover, the oscillator strengths of all the bands of the biferrocenyl products are larger than those of the monoferrocenyl compounds, suggesting a higher probability for π-π* and CT (ICT and MLCT) transitions in **BFc-TP** and **BFc-PIcm** compared with **Fc-TP** and **Fc-Icm** respectively. All of these facts indicate a larger π-conjugative effect in **BFc-TP** and **BFc-PIcm** than **Fc-TP** and **Fc-Icm**.

Electrochemistry

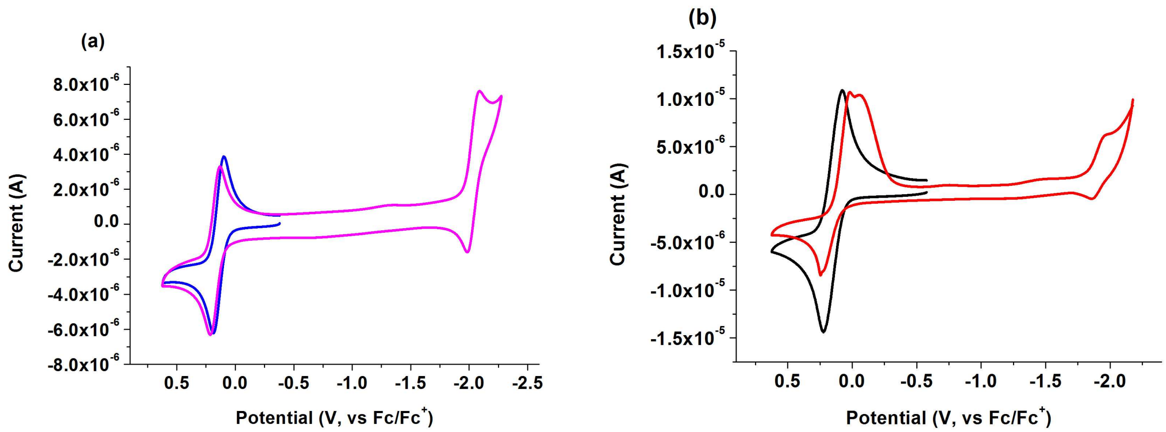

Fig. 4 Cyclic voltammograms of (a) **Fc-TP** (blue) and **Fc-Icm** (magenta) and (b) **BFc-TP** (black) and **BFc-PIcm** (red) in dichloromethane (20 °C, 1.0 mM of **Fc-TP**, **Fc-Icm**, **BFc-TP** and **BFc-PIcm**, 0.1 M TBAP, Pt disk as a working electrode, Ag/Ag^+ as a reference electrode, and Pt wire as a counter electrode, scan rate 100 mV/s).

Table 5 CV data of **Fc-TP, Fc-Icm, BFc-TP** and **BFc-PIcm** (vs Fc/Fc^+)

	$E_{1/2}$ (V)	E_{onset} (V)
Fc-TP	0.146	0.070
Fc-Icm	0.172	0.094
	-2.036	-1.969
BFc-TP	0.150	0.071
BFc-PIcm	0.078	0.081
	0.133	
	-1.910	-1.793

The electrochemical behavior of all compounds was surveyed by cyclic voltammetry. Cyclic voltammograms for **Fc-TP**, **Fc-Icm**, **BFc-TP** and **BFc-PIcm** are shown in **Fig. 4**. **Table 5** presents a summary of the potential data for the observed redox couples.

As shown in **Fig. 4**, monoferrcenyl compound **Fc-TP** exhibits one reversible redox wave at 0.146 V vs Fc/Fc^+ corresponding to the oxidation of ferrocenyl moiety, while **Fc-Icm** exhibits two redox waves, one reversible wave at 0.172 V vs Fc/Fc^+ due to the oxidation of ferrocenyl unit, and the other quasi-reversible wave at -2.036 V vs Fc/Fc^+ ascribing to the reduction of isocoumarin unit. All above can be supported by DFT calculations, since the orbital coefficient in HOMO is predominantly ferrocenyl-centered and that in LUMO is isocoumarin-centered (vide infra). In comparison with the E_{onset} of **Fc-TP** and **Fc-Icm**, it is clearly seen that the oxidation process of **Fc-Icm** is anodic shifted to higher potential, this can be attributed not only to the stereoelectronic aspect but also to the π-conjugative effect. On the one hand, better coplanarity is found in **Fc-Icm** than in **Fc-TP** (vide supra), which favors the π-orbital overlap and the orbital mixing. On the other hand, the ring closure leads to a remarkable increase in the π-conjugative system.

As for the biferrocenyl compound **BFc-TP**, only one redox process related to ferrocenyl moiety is observed ($E_{1/2}$ = 0.150 V vs Fc/Fc^+). But for **BFc-PIcm**, it exhibits two sequential irreversible waves at 0.078 and 0.133 V vs Fc/Fc^+, which may correspond to the stepwise oxidation of the two ferrocenyl units. At negative potential, it also displays the isocoumarin-centered reduction process around -1.910 V vs Fc/Fc^+. Similarly, from the potential of E_{onset}, it is clearly seen that the oxidation process of ferrocene-isocoumarin compond **BFc-PIcm** is also anodic shifted compared with **BFc-TP**, which could also be attributed to the π-conjugative effect. It is evident that **BFc-PIcm** is composed of more π-conjugative subunits and results in larger π-conjugative effect. Thus the stability of **BFc-PIcm** is better than that of **BFc-TP**. From the quantum-chemical calculations detailed below, the same result can also be obtained since **BFc-PIcm** has lower HOMO energy (vide infra). Therefore, the cyclization reaction results in weak electronic interactions between two ferrocenyl centers in **BFc-PIcm** and the more extending π-conjugated system may account for the anodic shift from **BFc-TP** to **BFc-PIcm**.

Computational study

In order to explain the difference in the UV-vis spectra as well as get insight into the electronic structures and the nature of all bands, DFT and TDDFT calculations were performed on the target compounds, which have been proven to provide reliable electronic structures, transition energies and intensities in a large variety of ferrocene derivatives.[17]

The HOMO and LUMO in the ground states of **Fc-TP**, **Fc-Icm**, **BFc-TP** and **BFc-PIcm** are shown in **Fig. 6,** and the main frontier orbitals related to different transitions are shown in **Fig. S7**. Molecular orbital energies and contributions analyzed with Multiwfn,[18,19] and vertical excitation energies of them, are detailed in **Table S4** and **S5**, respectively. The TDDFT predicted

UV-vis spectra of them are given in **Fig. S6**, which are in quite accordance with the experimental spectra. In agreement with their electronic structures, TDDFT calculations suggest the energy bands are mainly dominated by ICT, MLCT and π-π* transitions, which are elaborated in **Table S6**.

For all complexes, the calculated transitions qualitatively agree with the experimental ones. As for **Fc-TP**, the 464 nm band with a low value of *ε* corresponds to the transition calculated at 499 nm with a low oscillator strength *f*. This band is dominated by HOMO→LUMO transition. According to the orbital characters of the corresponding starting and arriving states (**Fig. 6** and **Table S4**), the HOMO is nearly Fe centered (76.41%), while the LUMO is predominately localized in the dimethyl terephthalate (TP) moiety (93.61%). The Fe characteristic HOMO and the TP characteristic LUMO indicate that this band bears a significant MLCT character. Another broad band appeared at 382 nm may be related to the calculated transition around 407 nm, which mainly originated from HOMO-2→LUMO. HOMO-2 is a ferrocenylethynyl centered orbital (86.83%), so this band is of ICT character. The intense 302 nm band may be related to four calculated bands around 338, 333, 329 and 295 nm (mainly 333 and 295nm), which mainly come from HOMO-5/HOMO-4→LUMO and HOMO/HOMO-1/HOMO-2→LUMO+1 transitions. From the involved orbital composition shown in **Table S4**, it is a mixed band with π-π*, MLCT and ICT character, which are detailed in **Table S6**. In addition, the most intense experimental band at 235 nm may correspond to the transitions calculated at 247 and 265 nm originating from HOMO-8→LUMO and HOMO-5/ HOMO-6→LUMO+1 MOs with strong oscillator strength, which is dominantly composed of several π-π* characteristic transitions. The percentage of each composition is clearly listed in **Table S6**.

As for **Fc-Icm**, analogous results are obtained from a TDDFT study. The low broad band found at 445 nm belongs to a MLCT transition originating from HOMO→LUMO calculated at 443 nm with low oscillator strength. The experimentally found band at 357 nm derives from two transitions with different features: 381 nm from HOMO-2→LUMO is of ICT character, and 337 nm from HOMO→LUMO+1 and HOMO→LUMO+3 are of MLCT and d-d character, respectively. Similar to the 302 nm band of **Fc-TP**, the intense band of **Fc-Icm** found at 311 nm relevant to three calculated transitions around 309, 306 and 305 nm with larger oscillator strength is a mixed band composed of a set of different transitions (HOMO-3/HOMO-4→LUMO, HOMO-2→LUMO+1) with π-π*, MLCT and ICT character. Moreover, the band found at 246 nm is also mainly attributed to the π-π* transition (HOMO-7→LUMO) calculated around 253 nm. The oscillator strength, composition and percentage of each transition are also given in **Table S6**. They are also in good agreement with the experimental results.

As for the biferrocenyl compound **BFc-TP**, a little difference can be found in the composition of the frontier orbitals and the oscillator strength since more π-conjugated units exist in it. Compared with the monoferrocenyl compound **Fc-TP** and **Fc-Icm**, it is obvious that the HOMO and LUMO of **BFc-TP** are more delocalized between Fc, -C≡C- and Tp moieties, and all the bands display stronger oscillator strength as shown in **Fig. 6**, **Table S4** and **Table S6**. As for the *cis*-**BFc-TP**, since only 50.16% of the HOMO's orbital composition is dedicated by Fe atoms, HOMO extends beyond ferrocenyl moiety all over *cis*-**BFc-TP**, and LUMO is predominantly consist of π* bonding (-C≡C-, TP), so the broad band found at 473 nm ascribing to the calculated 472 nm transition (HOMO→LUMO) is not a typical MLCT characteristic band, it is more likely to be considered as an ICT transition because HOMO is predominantly located in Fc and -C≡C- moiety (86.60%, **Table S4**), while LUMO is nearly TP centered (78.76%, **Table S4**). The experimental found 408 nm band is also of ICT character relevant to the calculated transition at 413 nm (HOMO-4→LUMO), and the experimental 336 nm band may be relevant to two calculated transitions at 349 (HOMO→LUMO+1) and 328 nm (HOMO-2→LUMO+1), which are of ICT and MLCT character, respectively. It is worth to note that the calculated MLCT transition at 328 nm with a lower oscillator strength *f* may be obscured by the strong ICT transition around 349 nm with an intense oscillator strength. Moreover, the calculated transition at 262 nm, which predominantly consists of HOMO-15→LUMO and HOMO-10→LUMO+1 π-π* transitions, and HOMO/HOMO-4→LUMO+5 d-d transitions, together with the calculated transition at 251 nm derived from HOMO-18→LUMO and HOMO-11→LUMO+4 with ICT and LMCT character, provides the major contribution to the experimental 247 nm. All the calculated results, including the oscillator strength, are excellently consistent with the experimental observations. Similarly results can be obtained for *trans*-**BFc-TP**, which can also be seen from **Fig. S7**, **Table S4** and **Table S6**.

Similarly, as for **BFc-PIcm**, three obvious bands (483, 372, 358 nm) are observed in the 300-600 nm region of the UV-vis absorption spectra, they can be attributed to ICT transitions relevant to the calculated transitions at 475 (HOMO→LUMO) and 402 (HOMO-4/HOMO→LUMO+1), 379 (HOMO/HOMO-4→LUMO+1) and 354 nm (HOMO-4→LUMO+1, HOMO→LUMO+5), respectively. At lower wavelength, the experimental 247 nm band consists of transitions calculated around 254 and 245 nm mainly with π-π*, LMCT and d-d character, which are elaborated in **Table S6**. Just as those discussed in **BFc-TP**, the calculated absorption bands in **BFc-PIcm** are also in good agreement with the experimental results.

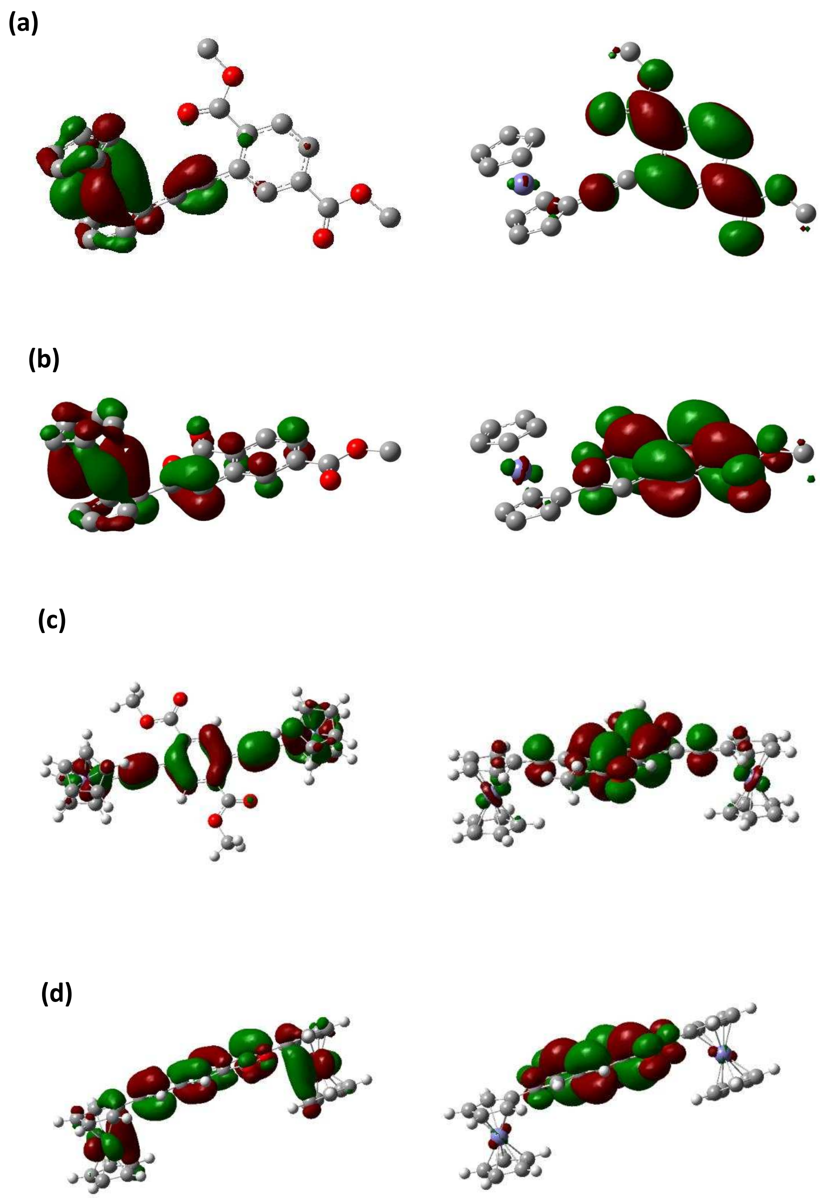

Fig. 6 HOMO (left) and LUMO (right) orbitals in the optimized ground-state structure of (a) **Fc-TP**, (b) **Fc-Icm**, (c) *cis*-**BFc-TP** and (d) *trans*-**BFc-PIcm**.

The calculated HOMO and LUMO energy levels of **Fc-TP**, **Fc-Icm**, **BFc-TP** and **BFc-PIcm** are listed in **Table 6**. The slightly higher HOMO energy levels of **Fc-TP** and **BFc-TP** compared with **Fc-Icm** and **BFc-PIcm** indicates that **Fc-TP** and **BFc-TP** are a little easier to lose electrons. These results are in good accordance with the experimental redox potentials. Therefore, the DFT calculations predict the experimentally observed trends in the redox properties of these compounds very well.

Table 6 Calculated DFT Energy Levels of Frontier Orbitals (eV) of **Fc-TP, Fc-Icm, BFc-TP** and **BFc-PIcm**.

Compound	HOMO	LUMO
Fc-TP	-5.43402	-2.48853
Fc-Icm	-5.77456	-2.53694
cis-**BFc-TP**	-5.43891	-2.48146
trans-**BFc-TP**	-5.43701	-2.48064
cis-**BFc-PIcm**	-5.68154	-2.64520
trans-**BFc-PIcm**	-5.67882	-2.64357

Conclusion

Two conjugative ferrocene-isocoumarin molecules **Fc-Icm** and **BFc-PIcm** are successfully prepared through acid catalytic intramolecular cyclization reactions from the corresponding ferrocenylethynyl terephthalates **Fc-TP** and **BFc-TP**. Single-crystal X-ray diffraction studies indicate the coplanarity of the two building blocks in **Fc-Icm** (Fc and ICM) is better than **Fc-TP** (Fc and Ph), and DFT calculations show that better coplanarity also exists in **BFc-TP** and **BFc-PIcm**. MLCT, ICT and π-π* absorption bands are found in the UV-vis spectra of all compounds, and the transitions of **BFc-TP** and **BFc-PIcm** are bathochromically shifted with larger oscillator strengths compared with **Fc-TP** and **Fc-Icm**. Electrochemical studies show that both **Fc-TP** and **BFc-TP** have only one reversible oxidation potential related to the ferrocenyl moiety, while **Fc-Icm** and **BFc-PIcm** undergo quasi/ir-reversible reduction process ascribing to the isocoumarin moiety besides the oxidation related to the ferrocenyl unit. Moreover, DFT and

TDDFT calculations are excellently consistent with the experimental data and clearly reflect the transition attributions and redox properties.

Acknowledgments

Authors thank National Nature Science Foundation of China for financial support (grant no. 51173075). In addition, we thank Dr Xing-Yong Wang for helpful discussions.

Electronic Supplementary Information (ESI)

CCDC 1060479 and 1060478 contain the supplementary crystallographic data for **Fc-TP** and **Fc-Icm**, respectively. These data can be obtained free of charge from The Cambridge Crystallographic Data Centre via www.ccdc.cam.ac.uk/data_request/cif. Packing structure and π-π interactions in **Fc-TP** and **Fc-Icm** are shown in Fig. S1 and S3, respectively. Hydrogen-bonding interactions in **Fc-TP** and **Fc-Icm** are shown in Fig. S2 and S4, respectively. Hydrogen bond distances and angles for **Fc-TP** and **Fc-Icm** are given in Table S1. Selected bond lengths and angles of **Fc-TP** and **Fc-Icm** predicted by DFT calculation are given in Table S2. TDDFT predicted UV-vis spectra of **Fc-TP**, **Fc-Icm**, **BFc-TP** and **BFc-PIcm** are shown in Fig. S5. Main frontier orbitals of them are shown in Fig. S6. Molecular orbital compositions of them are exhibited in Table S3. TDDFT predicted main vertical excitation energies for them are given in Table S4. For ESI and crystallographic data or other electronic format see DOI: ????????????????

References

1. (a) A. S. Blum, T. Ren, D. A. Parish, S. A. Trammell, M. H. Moore, J. G. Kushmerick, G. L. Xu, J. R. Deschamps, S. K. Pollack and R. Shashidhar, *J. Am. Chem. Soc.*, 2005, **127**, 10010; (b) W. W. Zhang, M. Kondo, T. Fujita, K. Namiki, M. Murata and H. Nishihara, *Molecules*, 2010, **15**, 150. (c) J. L. Delgado, E. Espíldora, M. Liedtke, A. Sperlich, D. Rauh, A. Baumann and C. Deibel, *Chem. Eur. J.*, 2009, **15**, 13474; (d) C. J. McAdam, B. H. Robinson, J. Simpson and T. Tagg, *Organometallics*, 2010, **29**, 2474; (e) A. Facchetti, *Chem. Mater.*, 2011, **23**, 733; (f) Y. Z. Wu and W. H. Zhu, *Chem. Soc. Rev.*, 2013, **42**, 2039; (g) C. Giansante, I. Infante, E. Fabiano, R. Grisorio, G. P. Suranna and G. Gigli, *J. Am. Chem. Soc.*, 2015, **137**, 1875; (h) T. Kusamoto, K.

Takada, R. Sakamoto, S. Kume and H. Nishihara, *Inorg. Chem.*, 2012, **51**, 12102.

2. (a) W. W. Zhang, Y. G. Yu, Z. D. Lu, W. L. Mao, Y. Z. Li and Q. J. Meng, *Organometallics*, 2007, **26**, 865. (b) W. Z. Yuan, Y. Y. Gong, S. M. Chen, X. Y. Shen, J. W. Y. Lam, P. Lu, Y. W. Lu, Z. M. Wang, R. R. Hu, N. Xie, H. S. Kwok, Y. M. Zhang, J. Z. Sun and B. Z. Tang, *Chem. Mater.*, 2012, **24**, 1518; (c) L. Y. Lin, Y. H. Chen, Z. Y. Huang, H.W. Lin, S. H. Chou, F. Lin, C. W. Chen, Y. H. Liu and K. T. Wang, *J. Am. Chem. Soc.*, 2011, **133**, 15822; (d) S. G. Esteban, P. de la Cruz, A. Aljarilla, L. M. Arellano and F. Langa, *Org. Lett.*, 2011, **13**, 5362; (e) K. Vandewal, S. Albrecht, E. T. Hoke, K. R. Graham, J. Widmer, J. D. Douglas, M. Schubert, W. R. Mateker, J. T. Bloking, G. F. Burkhard, A. Sellinger, J. M. J. Frechet, A. Amassian, M. K. Riede, M. D. McGehee, D. Neher and A. Salleo, *Nat. Mater.*, 2014, **13**, 63; (f) H. Zhu, Y. Z. Wu, J. C. Liu, W. W. Zhang, W. J. Wu and W. H. Zhu, *J. Mater. Chem. A.*, 2012, **00**, 1; (g) D. B Zhang, J. Y. Wang, H. M. Wen and Z. N. Chen, *Organometallics*, 2014, **33**, 4738; (h) S. Muratsugu, M. Kishida, R. Sakamoto and H. Nishihara, *Chem. Eur. J.*, 2013, **19**, 17314. (i) G. T. Xu, B. Lin, J. Y. Wang, D. B. Zhang and Z. N. Chen, *Chem. Eur. J.*, 2015, **21**, 3318.

3. (a) K. M. Roth, A. A. Yasseri, Z. M. Liu, R. B. Dabke, V. Malinovskii, K-H. Schweikart, L. H. Yu, H. Tiznado, F. Zaera, J. S. Lindsey, W. G. Kuhr and D. F. Bocian, *J. Am. Chem. Soc.*, 2003, **125**, 505; (b) O. Azzaroni, M. Álvarez, A. I. Abou-Kandil, B. Yameen and W. Knoll, *Adv. Funct. Mater.*, 2008, **18**, 3487; (c) Z. S. Wu, M. M. Guo, S. B. Zhang, C. R. Chen, J. H. Jiang, G. L. Shen and R. Q. Yu, *Anal. Chem.*, 2007, **79**, 2933; (d) J. S. Marois and J. F. Morin, *Langmuir*, 2008, **24**, 10865; (e) J. Tang, D. P. Tang, R. Niessner, G. N. Chen and D. Knopp, *Anal. Chem.*, 2011, **83**, 5407; (f) S. J. Wang, Y. F. Wang and C. X. Cai, *J. Phys. Chem. C*, 2015, **119**, 5589; (g) T. L. Kinnibrugh, S. Salman, Y. A. Getmanenko, V. Coropceanu, W. W., III Porter, T. V. Timofeeva, A. J. Matzger, J. L. Brédas, S. R. Marder and S. Barlow, *Organometallics*, 2009, **28**, 1350; (h) W. A. Amer, L. Wang, A. M. Amin, L. Ma and H. Yu, *J. Inorg. Organomet. Polym.*, 2010, **20**, 605; (i) R. Horikoshi and T. Mochida, *Eur. J. Inorg. Chem.*, 2010, 5355.

4. (a) Y. Fan, I. P-C. Liu, P. E. Fanwick and T. Ren, *organometallics*, 2009, **28**, 3959; (b) T. L. Kinnibrugh, S. Salman, Y. A. Getmanenko, V. Coropceanu, W. W., III Porter, T. V. Timofeeva, A. J. Matzger, J. L. Brédas, S. R. Marder and S. Barlow, *Organometallics*, 2009, **28**, 1350; (c) W. A. Amer, L. Wang, A. M. Amin, L. Ma and H. Yu, *J. Inorg. Organomet. Polym.*, 2010, **20**, 605; (d) R. Horikoshi and T. Mochida, *Eur. J. Inorg. Chem.*, 2010, 5355; (e) C. J. Ziegler, K. Chanawanno, A. Hasheminsasab, Y. V. Zatsikha, E. Maligaspe and V. N. Nemykin, *Inorg.*

Chem., 2014, **53**, 4751; (f) Y. L. Rao, T. Kusamoto, R. Sakamoto, H. Nishihara and S. N. Wang, *Organometallics*, 2014, **33**, 1787.

5. (a) C. Prompanya, T. Dethoup, L. J. Bessa, M. M. M. Pinto, L. Gales, P. M. Costa, A. M. S. Silva and A. Kijjoa, *Mar. Drugs*, 2014, **12**, 5160; (b) Y. Lu, D. S. Leow, X. S. Wang, K. M. Engle and J. Q. Yu, *Chemical Science*, 2011, **2**, 967; (c) S. P. Waters and M. C. Kozlowski, *Tetrahedron Letters*, 2001, **42**, 3567; (d) K. Krohn, I. Kock, B. Elsässer, U. Flörke, B. Schulz, S. Draeger, G. Pescitelli, S. Antus and T. Kurtán, *Eur. J. Org. Chem.*, 2007, 1123.

6. (a) J. C. Powers, J. L. Asgian, O. D. Ekici and K. E. James, *Chem. Rev.*, 2002, **102**, 4639. (b) K. M. Khan, S. Ahmed, Z. A. Khan, M. Rani, S. Perveen and W. Voelter, *Nat. Prod. Res.*, 2008, **22**, 1120. (c) K. Nozawa, M. Yamada, Y. Tsuda, K. Kawai and S. Nakajima, *Chem. Pharm. Bull.* 1981, **29**, 2689; (d) D. Engelmeier, F. Hadacek, O. Hofer, G. Lutz-Kutschera, M. Ngl, G. Wurz and H. Greger, *J. Nat. Prod.*, 2004, **67**, 19; (e) M. E. Riveiro, A. Moglioni, R. Vazquez, N. Gomez, G. Facorro, L. Piehl, E. R. De Celis, C. Shayo and C. Davio, *Bioorg. Med. Chem.*, 2008, **16**, 2665; (f) Y. Shikishima, Y. Takaishi, G. Honda, M. Ito, Y. Takeda, O. K. Kodzhimatov, O. Ashurmetov and K. H. Lee, *Chem. Pharm. Bull.*, 2001, **49**, 877; (g) J. J. Heynekamp, L. A. Hunsaker, T. A. Vander Jagt, R. E. Royer, L. M. Deck and D. L. Vander Jagt, *Bioorg. Med. Chem.*, 2008, **16**, 5285.

7. (a) R. K. Chinnagolla and M. Jeganmohan, *Chem. Commun.*, 2012, **48**, 2030; (b) M. R. Kumar, F. M. Irudayanathan, J. H. Moon and S. W. Lee, *Adv. Synth. Catal.*, 2013, **355**, 3221; (c) X.-X. Guo, *J. Org. Chem.*, 2013, **78**, 1660; (d) Y. He, X. Y. Zhang, N. N. Shen and X. S. Fan, *J. Org. Chem.*, 2013, **78**, 10178; (e) U. Haedke, M. Götz, P. Baer and S. H. L. Verhelst, *Bioorg. Med. Chem.*, 2012, **20**, 633; (d) M. Uchiyama, H. Ozawa, K. Takuma, Y. Matsumoto, M. Yonehara, K. Hiroya and T. Sakamoto, *Org. Letters*, 2006, **8**, 5517.

8. V. Benin, S. Durganala and A. B. Morgan, *J. Mater. Chem.*, 2012, **22**, 1180.

9. (a) N. Ivan, V. Benin and A. B. Morgan, *Synth. Commun.*, 2013, **43**, 1831; (b) R. J.Perry and B. D. Wilson, *Macromolecules*, 1995, **28**, 3509; (c) Q. Zhou and T. M. Swager, *J. Am. Chem. Soc.*, 1995, **117**, 12593.

10. A. D. Becke, *J. Chem. Phys.*, 1993, **98**, 5648.

11. C. Lee, W. Yang and R. G. Parr, *Phys. Rev. B*, 1988, **37**, 785.

12. P. J. Hay and W. R. Wadt, *J. Chem. Phys.*, 1985, **82**, 299.

13. Gaussian 09, Revision **A.1**, M. J. Frisch, G. W. Trucks, H. B. Schlegel, G. E. Scuseria, M. A.

Robb, J. R. Cheeseman, G. Scalmani, V. Barone, B. Mennucci, G. A. Petersson, H. Nakatsuji, M. Caricato, X. Li, H. P. Hratchian, A. F. Izmaylov, J. Bloino, G. Zheng, J. L. Sonnenberg, M. Hada, M. Ehara, K. Toyota, R. Fukuda, J. Hasegawa, M. Ishida, T. Nakajima, Y. Honda, O. Kitao, H. Nakai, T. Vreven, J. A. Montgomery, Jr., J. E. Peralta, F. Ogliaro, M. Bearpark, J. J. Heyd, E. Brothers, K. N. Kudin, V. N. Staroverov, R. Kobayashi, J. Normand, K. Raghavachari, A. Rendell, J. C. Burant, S. S. Iyengar, J. Tomasi, M. Cossi, N. Rega, J. M. Millam, M. Klene, J. E. Knox, J. B. Cross, V. Bakken, C. Adamo, J. Jaramillo, R. Gomperts, R. E. Stratmann, O. Yazyev, A. J. Austin, R. Cammi, C. Pomelli, J. W. Ochterski, R. L. Martin, K. Morokuma, V. G. Zakrzewski, G. A. Voth, P. Salvador, J. J. Dannenberg, S. Dapprich, A. D. Daniels, O. Farkas, J. B. Foresman, J. V. Ortiz, J. Cioslowski and D. J. Fox, Gaussian, Inc., Wallingford CT, 2009.

14. *Software packages SMART and SAINT*, Siemens Analytical X-ray Instrument Inc., Madison, WI, 1996.

15. G. M. Sheldrick, *SHELX–97*, *Program for the refinement of crystal structure*, University of Göttingen, Germany, 1997.

16. (a) T. Shoji, A. Maruyama, C. Yaku, N. Kamata, S. Ito, T. Okujima and K. Toyota, *Chem. Eur. J.*, 2015, **21**, 402; (b) Á. Díez, J. Fernández, E. Lalinde, M. T. Moreno and S. Sánchez, *Dalton Tran*., 2008, **36**, 4926; (c) Á. Díez, J. Fernández, E. Lalinde, M. T. Moreno and S. Sánchez, *Dalton Tran*., 2009, **18**, 3434.

17. (a) P. V. Solntsev, S. V. Dudkin, J. R. Sabin and V. N. Nemykin, *Organometallics*, 2011, **30**, 3037; (b) V. N. Nemykin and R. G. Hadt, *J. Phys. Chem. A*, 2010, **114**, 12062; (c) F. Fabrizi de Biani, G. Manca, L. Marchetti, P. Leoni, S. Bruzzone, C. Guidotti, A. Atrei, A. Albinati and S. Rizzato, *Inorg. Chem.*, 2009, **48**, 10126; (d) Y. L. Li,; L. Han, Y. Mei, J. Z. H. Zhang, *Chem. Phys. Lett.*, 2009, **482**, 217.

18. T. Lu and F. W. Chen, *J. Comp. Chem.*, 2012, **33**, 580.

19. T. Lu and F. W. Chen, *Acta Chim. Sinica*, 2011, **69**, 2393.